THE JOURNAL OF PHYSICAL CHEMISTRY C

Article

Cite This: J. Phys. Chem. C 2018, 122, 12090−12097

pubs.acs.org/JPCC

The Evolution of Intermolecular Energy Bands of Occupied and Unoccupied Molecular States in Organic Thin Films

Yuki Kashimoto,[†] Keiichirou Yonezawa,[‡] Matthias Meissner,[‡,§] Marco Gruenewald,[§] Takahiro Ueba,[‡] Satoshi Kera,[*,†,‡] Roman Forker,[§] Torsten Fritz,[*,§] and Hiroyuki Yoshida[*,†,∥]

[†]Graduate School of Engineering, Chiba University, 1-33, Yayoi-cho, Inage-ku, Chiba 263-8522, Japan

[‡]Institute for Molecular Science, Myodaiji, Okazaki, 444-8585, Japan

[§]Institut für Festkörperphysik, Friedrich-Schiller-Universität Jena, Helmholtzweg 5, 07743 Jena, Germany

[∥]Molecular Chirality Research Center, Chiba University, 1-33, Yayoi-cho, Inage-ku, Chiba 263-8522, Japan

Supporting Information

ABSTRACT: In organic semiconductors, the hole and electron transport occurs through the intermolecular overlaps of highest occupied molecular orbitals (HOMO) and lowest unoccupied molecular orbitals (LUMO), respectively. A measure of such intermolecular electronic coupling is the transfer integral, which can experimentally be observed as energy level splittings or the width of the respective energy bands. Quantum chemistry textbooks describe how an energy level splits into two levels in molecular dimers, into three levels in trimers and evolves into an energy band in infinite systems, a process that has never been observed for the LUMO or beyond dimers for the HOMO. In this work, our new technique, low-energy inverse photoelectron spectroscopy, was applied to observe the subtle change of the spectral line shape of a LUMO-derived feature while we used ultraviolet photoelectron spectroscopy to investigate the occupied states. We show at first that tin-phthalocyanine molecules grow layer-by-layer in quasi-one-dimensional stacks on graphite, and then discuss a characteristic and systematic broadening of the spectral line shapes of both HOMO and LUMO. The results are interpreted as energy-level splittings due to the intermolecular electronic couplings. On the basis of the Hückel approximation, we determined the transfer integrals for HOMO−1, HOMO, and LUMO to be ≤15 meV, (100 ± 10) meV, and (128 ± 10) meV, respectively.

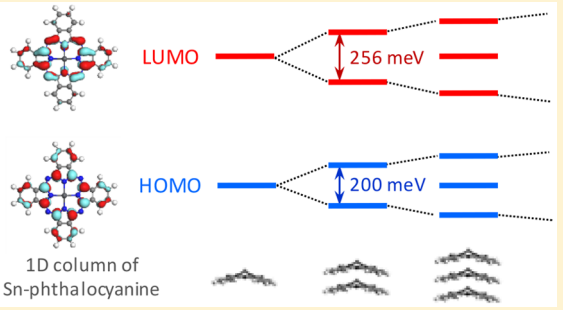

1. INTRODUCTION

Since the middle of the last century, the transport mechanisms in organic semiconductors have been a central and sometimes controversially discussed research topic. The charge carrier transport is determined by the intermolecular overlap of π-orbitals of the constituent molecules.[1] A good measure of the intermolecular orbital overlap is the bandwidth of the resulting bands and the transfer integral t between the orbitals involved. In the early stage of research, the bandwidths of organic solids were believed to be a few tens of millielectronvolts at maximum.[2] Since the 1990s, however, k-resolved ultraviolet photoelectron studies showed intermolecular energy band dispersions with the bandwidth exceeding 0.1 eV in organic solids[3] and later on small bandwidths less than 0.1 eV were observed.[4]

While the bandwidths can be obtained experimentally via photoelectron spectroscopies, the transfer integral t is the primary parameter for the theoretical treatment of carrier transport. In organic solids, the transfer integral is connected with the bandwidth (or the energy level splitting) in the framework of the tight-binding approximation, when the molecular orbital is taken as a basis (and not atomic orbitals, as in inorganic solids). Further, here the transfer integrals of only the nearest-neighbor molecules are taken into consideration and the overlap integrals are ignored, which is referred to as the Hückel approximation, as it is conceptually equivalent to the treatment of atomic orbitals in the Hückel LCAO (linear combination of atomic orbitals). The simplest example is a one-dimensional molecular chain. When two molecules approach each other, every energy level splits into two with an energy difference $2t$, where t will be different for the different energy levels and may even become zero. Three and four molecules generate three and four levels, respectively, and if the molecular chain length approaches infinity, the separation of energy levels becomes increasingly close until a one-dimensional band with a continuous density of states is formed as schematically shown in Figure 1.[5] Therefore, we will refer to our model in the following as Hückel model for short.

Although a calculated dimer splitting of $2t$ is often used to determine the transfer integral as described in the theory of

Received: March 16, 2018
Revised: April 19, 2018
Published: April 24, 2018

DOI: 10.1021/acs.jpcc.8b02581
J. Phys. Chem. C 2018, 122, 12090−12097

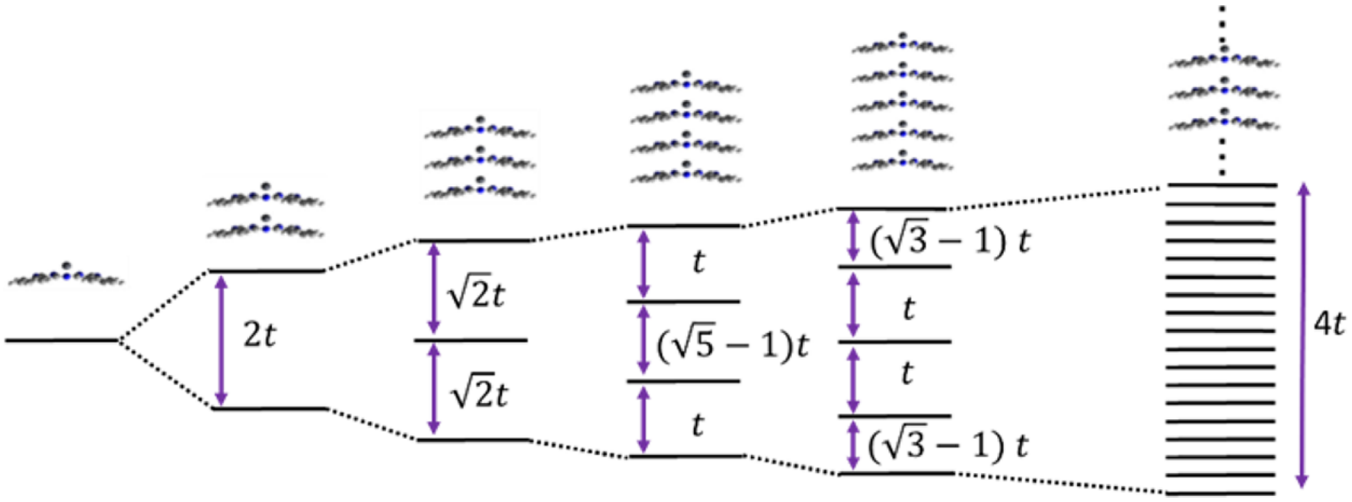

Figure 1. Energy splittings due to intermolecular orbital interaction. The energy separations are based on the Hückel approximation using the transfer integral *t*. For increasing chain lengths, the bandwidth approaches the value of an infinite chain, being 4*t*.

organic semiconductors,[1] an experimental observation of the splitting is much more challenging than measuring the band dispersion because it requires precise control of the uniformity and the number of layers in the film, in addition to preparing a film with a desired crystal structure and molecular orientation, as the transfer integral depends rather sensitively on the molecular alignment.[6,7] In 2007, Kera et al. demonstrated that splitting of the highest occupied molecular orbital (HOMO) occurs in a bilayer of lead-phthalocyanine (PbPc) and derived a transfer integral of 175 meV at 295 K.[8]

Most studies published so far focus only on the hole transport based on the intermolecular orbital interaction of HOMO-derived levels. In fact, no experimental data are available for the intermolecular orbital overlap of LUMO-derived levels. In a bipolar semiconductor device such as an organic light emitting diode or an organic photovoltaic cell, however, not only the hole but also the electron plays a central role for its performance. The intermolecular orbital interaction of the lowest unoccupied molecular orbitals (LUMO) is responsible for electron conduction. Although intermolecular interaction between LUMOs is often assumed to be similar to that between HOMOs, this assumption can be challenged for the following reasons: (i) The shapes of HOMO and LUMO wave functions are different. For example, the number of nodes is larger in the LUMO than in the HOMO, leading to a smaller transfer integral for the LUMO. (ii) Quite oppositely, the spatial extensions are different for occupied and unoccupied molecular orbitals because a charge carrier in the LUMO (excess electron) and a hole in the HOMO (electron deficiency) may increase and reduce the shielding of the positive charge of atomic cores, respectively, leading to a LUMO transfer integral that is larger than that of the HOMO. Therefore, the LUMO's transfer integral may be larger or smaller than the HOMO's, depending on which effect is stronger, but at least it will most likely be different. Furthermore, most organic semiconductors predominantly show hole conduction, and developing an "n-type" semiconductor with high electron mobility has been a central issue in organic electronics.[9,10] Therefore, understanding the electron conduction via the LUMO is both interesting and challenging at the same time.

The main reason for the nonexistence of experimental data for the LUMO transfer integral is a lack of suitable experimental methods for unoccupied states of organic semiconductors. Although the optical transition from HOMO to LUMO, employing UV−vis absorption spectroscopy or two-photon photoelectron spectroscopy, is often used to estimate the LUMO-derived levels indirectly (problems may arise from the exciton binding energy which is not known in most cases[11−13]), the entire energy level splitting caused by the intermolecular interaction cannot be deduced due to the selection rule governing optical excitations. In principle, the ideal method would be inverse photoelectron spectroscopy (IPES) which detects a photon emitted due to the transition of an impinging electron from the free-electron state to an unoccupied state in the solid and which is able to probe all the split levels. Yet, conventional IPES[14] is not precise enough to measure the intermolecular electronic coupling. The typical energy resolution is 0.5 eV, already exceeding the expected intermolecular interaction energy of the order of 100 meV, and the electron bombardment may damage organic samples[15,16] leading to a poor signal-to-noise ratio if appropriate low electron intensities are applied.

Recently we have developed an experimental technique called low-energy inverse photoelectron spectroscopy (LEIPS).[17−19] In this technique, the electron energy is lower than the damage threshold of organic molecules[20] to avoid the damage of organic samples. The obtained spectra possess a high signal-to-noise ratio allowing for the analysis of splittings of the LUMO-derived peak. By lowering the electron energy, the emitted photon is in the near-ultraviolet range, which can be analyzed using a high resolution bandpass filter. As a result, an overall resolution of as good as 0.25 eV was attained.[19]

In this study, we experimentally demonstrate the splittings of both HOMO- and LUMO-derived levels in a quasi-one-dimensional arrangement. At first, we show that tin-phthalocyanine (SnPc) grows in a layer-by-layer fashion on graphite producing quasi-one-dimensional columns. Then, the splittings of HOMO and LUMO-derived levels evolving into the one-dimensional band structure are observed using ultraviolet photoelectron spectroscopy (UPS) and LEIPS, respectively, for film thicknesses from 1 to 5 monolayers.

DOI: 10.1021/acs.jpcc.8b02581
J. Phys. Chem. C 2018, 122, 12090−12097

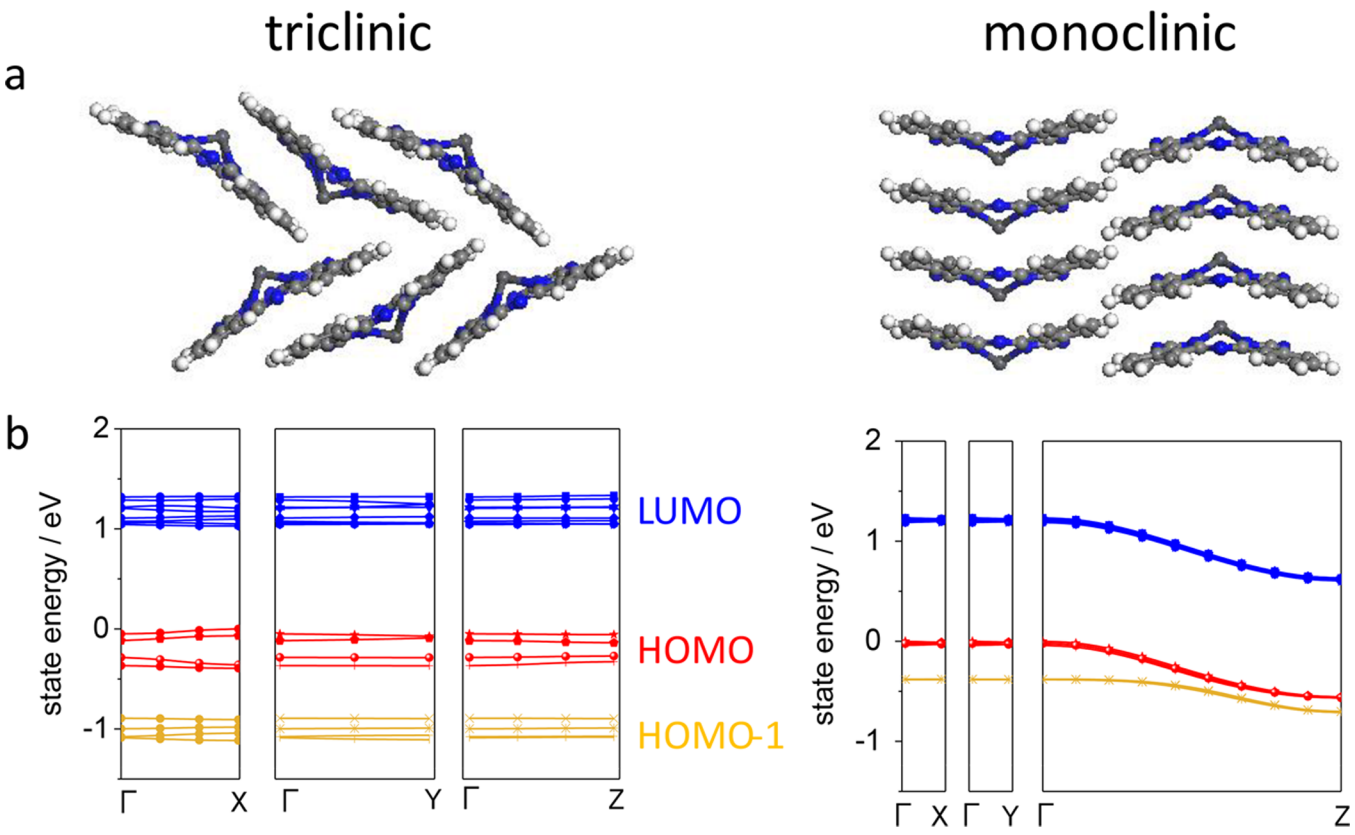

Figure 2. (a) Molecular alignment in the (001) plane of the triclinic[28] and the (100) plane of the monoclinic[27] crystal phases of PbPc and (b) the corresponding calculated band structures.

Analyzing the data, we evaluate the transfer integrals for both the HOMO and LUMO-derived levels.

2. METHODS

The electronic properties of the SnPc films were measured in Chiba and Okazaki, Japan, using UPS and LEIPS. For this, sublimed-grade SnPc was purchased from NARD Chemicals Ltd. and used as received. As a substrate, highly oriented pyrolytic graphite (HOPG, SPI-1 grade) was cleaved in air, and the surface was cleaned by heating in vacuum (10^{-7} Pa) at 673 K over 12 h. SnPc was vacuum-deposited onto the HOPG substrate kept at room temperature and afterward annealed at 373 K for 1 h, then cooled to room temperature at the natural cooling rate. The average film thickness and deposition rate (0.05−0.10 nm min^{-1}) were monitored using a quartz microbalance. Completion of the first monolayer (ML) was determined as disappearance of specific peaks derived from the image potential and from σ^* states of HOPG in LEIPS and metastable atom electron spectroscopy (MAES), respectively. The in situ UPS and LEIPS measurements were conducted in separate vacuum chambers.

For UPS, a HeI light source with a photon energy of 21.218 eV was incident to the sample film kept at room temperature, and the normal emission was detected using a PHOIBOS 100 analyzer (SPECS) with a pass energy of 3 eV and an acceptance angle of ±3° in Chiba and a DA30 analyzer (ScientaOmicron) in Okazaki. The total resolution was better than 50 and 20 meV, respectively. The LEIPS experiments were carried out in Chiba. Details of the LEIPS apparatus are described elsewhere.[21] In short, the electron beam with a current of 0.3 μA is incident to the sample along the surface normal, and the emitted photons were analyzed using a bandpass filter (having a center energy of 4.45 eV and a width of 0.17 eV) and a photomultiplier. In order to avoid sample damage due to the electron bombardment, the kinetic energy of the incident electron beam was kept below 5 eV. The energy and angular spread of the electrons were 0.25 eV and 5°, respectively. The overall energy resolution which is determined by the convolution of the electron energy spread and the width of the bandpass filter was about 0.3 eV. Typical measurement time was 2 h, and no discernible alterations of the spectra due to sample damage were observed.

The crystal structure of the SnPc films was examined in Jena, Germany, using distortion-corrected and calibrated low-energy electron diffraction (LEED)[22] as well as differential reflectance spectroscopy (DRS).[23,24] For those experiments, SnPc was provided by Achim Schöll and Christoph Sauer (Würzburg University), purified by gradient sublimation and deposited on single-crystal graphite (obtained from Naturally Graphite, Michigan Technological University). For DRS, light from a 100 W halogen lamp operated with a stabilized power supply (Müller Elektronik-Optik) is incident to the sample under 20°, measured to the surface normal. The reflected light is then spectrally analyzed by means of a monochromator (Acton Research SpectraPro SP2356) and a charge-coupled device (CCD; Princeton Instruments Spec-10 100BR, liquid-nitrogen-cooled). The measured quantity, the relative change of reflectance during film deposition, is then used to extract the complex dielectric function $\varepsilon(E,d) = \varepsilon'(E,d) - i\varepsilon''(E,d)$ depending on the photon energy E and film thickness d, as described elsewhere.[23] After the preparation of SnPc films with varying thicknesses, LEED experiments were performed at

DOI: 10.1021/acs.jpcc.8b02581
J. Phys. Chem. C 2018, 122, 12090−12097

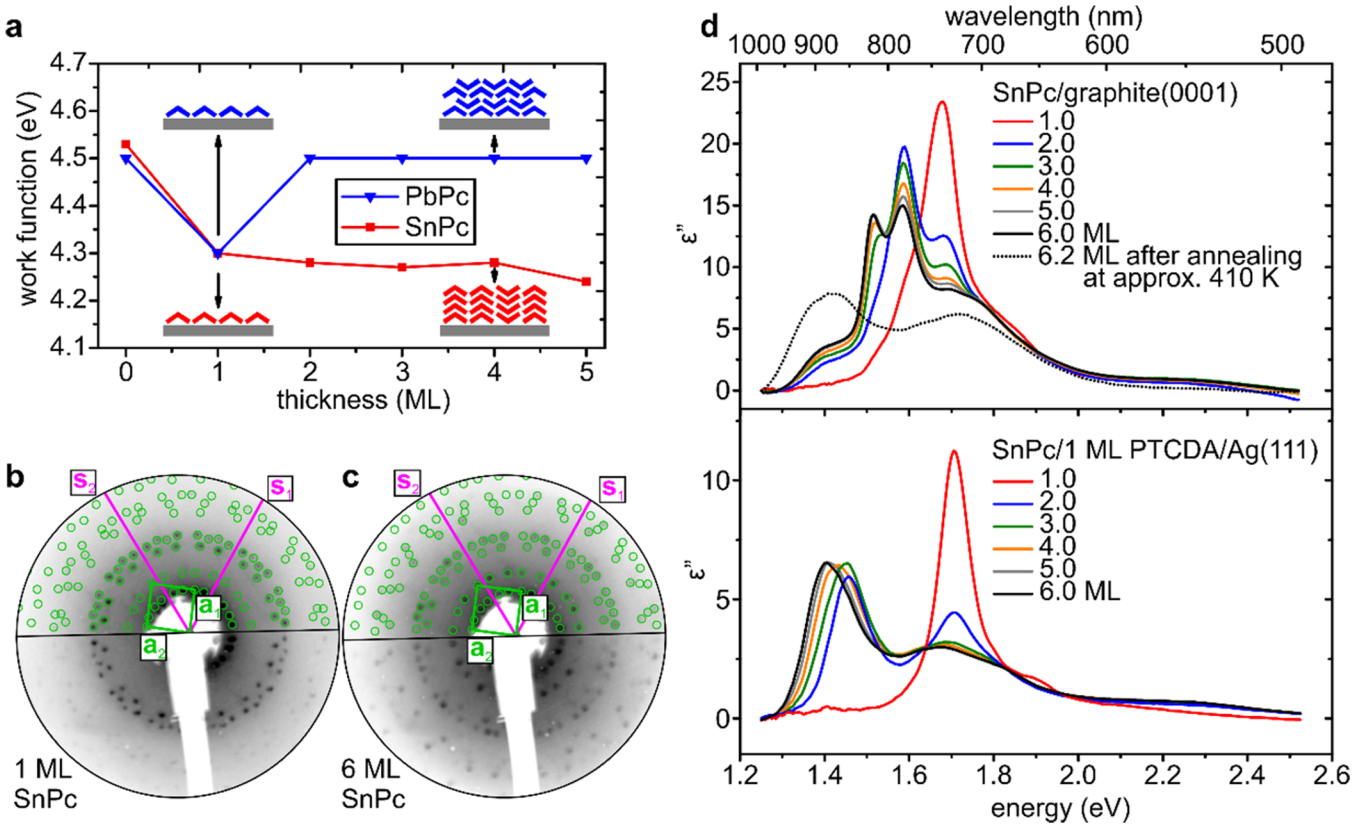

Figure 3. (a) Workfunctions of SnPc and PbPc films as a function of the number of layers. (b,c) LEED patterns of 1 and 6 ML SnPc on graphite, respectively (contrast logarithmic, inverted). The electron energies were 35.5 eV. The direction of the substrate unit cell vectors is indicated in magenta, diffraction orders due to SnPc are marked in green. (d) Thickness-dependent imaginary part ε'' of the dielectric function of SnPc on graphite during deposition and after annealing at 410 K, respectively (top panel), compared to triclinic SnPc on 1 ML PTCDA on Ag(111) (bottom panel[36]).

room temperature using a dual microchannel plate LEED from OCI Vacuum Microengineering. To achieve quantitative LEED measurements the images were corrected regarding distortions of the raw data, by applying a previously published algorithm,[22,25] and subsequently analyzed using the software LEEDLab.[26]

Throughout the paper, our measurements on SnPc films will be compared to previous ones using the similar, shuttlecock-shaped PbPc molecule. The multitude of data on the structure of PbPc crystals and films helps to understand the structural properties of our samples. Therefore, an energy band calculation of PbPc was performed for the single crystal structures[27,28] using DMol3 code on the Material Studio program (Accelrys). The Perdew–Burke–Ernzerhof (PBE) functional of the generalized gradient approximation (GGA) with the DNP (double-numeric quality basis set + d-polarization functions for heavy atoms + p-polarization functions for hydrogen atoms) basis set was used. The molecular orbitals of a single SnPc molecule were calculated using the Becke three-parameter Lee–Yang–Parr exchange-correlation (B3LYP) functional with basis sets of Los Alamos ECP plus MBS for Sn and STO-3G for other atoms in the Gaussian 09 software.[29]

3. RESULTS AND DISCUSSION

3.1. Film Structure. In order to observe the development of energy level splittings as schematically shown in Figure 1, it is necessary to prepare a film consisting of one-dimensional columns containing controlled numbers of molecules. Further, the intermolecular interaction must be large within the columns but negligibly small between the columns.

Planar phthalocyanines often crystallize into one-dimensional columns. However, the intermolecular orbital overlap is poor, and the transfer integral along the stack is as small as 30 meV.[4] Therefore, we used a shuttlecock-shape phthalocyanine instead because of the larger intermolecular interaction along the stacking direction. For example, the monoclinic phase of PbPc consists of molecular stacks forming linear columns parallel to the *c*-axis and exhibits high conductivity along this axis.[27] In fact, the energy band calculation shows a large sinusoidal dispersion only along the *c*-axis as shown in Figure 2, characteristic of one-dimensional conductors. The other known polymorph of PbPc is a triclinic phase where the molecules stack with their convex and concave sides alternatingly pointing up.[28] In that case, however, the energy band splits in two sub-bands and the dispersion is small (Figure 2b), indicating a strong dimer interaction within the unit cell.

Another requirement for this study is that the substrate should be conductive to avoid the charging of the sample during the electron spectroscopies, while the interaction between the substrate and the molecules should be small. This is almost ideally fulfilled by graphite. If a thin film with a molecular arrangement similar to the monoclinic phase of PbPc were to grow layer-by-layer with the stack axis normal to the substrate, that is, with the molecular plane parallel to the substrate surface, the evolution of the band structure could be

DOI: 10.1021/acs.jpcc.8b02581
J. Phys. Chem. C 2018, 122, 12090–12097

observed using both UPS and LEIPS. Yet, so far monoclinic PbPc films are only reported to grow on polycrystalline Au[30] and CuI[31] surfaces but unfortunately with an edge-on molecular orientation. Further, the molecule−substrate interaction can be expected to be fairly large in those cases. Nevertheless, using the similar shuttlecock phthalocyanine SnPc, we identify a suitable structure in layer-by-layer grown films in which one-dimensional columns align indeed normal to the substrate.

Figure 3a compares the workfunction of PbPc and SnPc films on HOPG as a function of film thickness. The workfunction decreases until the completion of the first monolayer in both systems and then increases in the case of PbPc while continuing to decrease with higher layers of SnPc at a slower pace. PbPc and SnPc possess permanent electric dipoles normal to the Pc ring. Thus, the different behavior can be traced back to different molecular orientations. PbPc orients with the concave side down in the first monolayer and then upside down in the second layer to avoid building up a permanent dipole moment in the bilayer.[8] On the other hand, the different behavior of SnPc indicates that the molecules stack in a different manner because the built-up surface dipole of the first ML is retained and slowly increased in thicker layers.

In order to reveal the crystallographic structure of the SnPc film, LEED measurements were performed and the results are shown in Figure 3b,c. The two-dimensional lattice parameters are summarized in Table 1 and compared with those from X-ray diffraction on single crystals.[27,28,32] In the first monolayer, the SnPc film adopts the same structure as 1 ML of PbPc on graphite. However, while PbPc was concluded to form a structure on graphite similar to its triclinic polymorph,[8] subsequent layers of SnPc form almost-square unit cells that cannot be found in the triclinic crystal structure of SnPc or PbPc. Furthermore, the surface lattice parameters of a 6 ML SnPc film are similar to the (001) plane of the monoclinic PbPc polymorph[27] in the sense that the lattice constants a_1 and a_2 are almost identical to each other and the angle between the $\boldsymbol{a}_1$ and $\boldsymbol{a}_2$ vectors is nearly 90°. These findings strongly suggest that the SnPc film on graphite is similar to the monoclinic phase of PbPc and that the SnPc molecules arrange in quasi-one-dimensional stacks. However, in contrast to the monoclinic PbPc structure which includes four molecular columns (two with upward-facing molecules and two with opposite orientation), the SnPc lattice constants allow for only one molecular stack in the unit cell. While this by itself would mean that all SnPc columns face the same direction, the continued built-up of a surface dipole due to such a uniform arrangement is excluded by the thickness-dependent change of the workfunction, which slows down significantly after the completion of the first ML. The apparent contradiction can be solved by assuming that a random mixture of upward- and downward-facing columns coexist. This is consistent with deviations from long-range order in the up/down orientation of molecules reported for monoclinic PbPc crystals.[27] Moreover, this effect does not render our conclusions about the electronic structure invalid, as we will discuss later. Note also that our structure stands out because even though there are many reports of SnPc film structures, such as for SnPc on HOPG(0001),[33] Ag(111),[34,35] and 1 ML PTCDA/Ag(111),[36] a monoclinic-like unit cell has not been reported so far for SnPc.

Table 1. Lattice Constants of PbPc and SnPc Films on Graphite and in Single Crystals

	a_1 (Å)	a_2 (Å)	$\angle(\boldsymbol{a}_1, \boldsymbol{a}_2)$ (deg)
PbPc 1 ML[39]	13.8(2)	13.9(2)	92.1(1)
SnPc 1 ML	13.8(3)	13.9(3)	91.7(1)
SnPc 2 ML	13.7(1)	13.7(1)	90.4(1)
SnPc 6 ML	13.64(13)	13.65(13)	90.1(1)
(001) plane of monoclinic PbPc[a]	25.48[d]	25.48[d]	90
(010) plane of triclinic PbPc[b]	13.12	12.89	96.20
(10$\bar{1}$) plane of triclinic SnPc[c]	12.62	14.22	104.64

[a]Reference 27. [b]Reference 28. [c]Reference 32. [d]The unit cell contains two upward facing and two downward facing molecular columns.

In order to further validate the structure, optical absorption spectroscopy shall be briefly discussed, because it is sensitive to the molecular packing and is an established method to identify different polymorphs of phthalocyanines.[31,36,37] In the case of PbPc, the Q-band of monomers is observed around 1.68 eV.[38] The absorption maximum redshifts only slightly to 1.65 eV in monoclinic PbPc, while in the triclinic phase the band splits strongly and the main peak is observed at 1.35 eV representing a large red-shift of 0.4 eV.[30] Likewise, a triclinic-like SnPc thin film[36] has been reported to feature the strongest absorption around 1.37 eV.

We measured the optical absorption of the Q-band region of SnPc thin films on graphite as a function of film thickness using in situ DRS as shown in Figure 3d. In the submonolayer range, the SnPc spectra are dominated by a main peak at 1.7 eV assignable to the monomeric SnPc Q-band and a high-energy shoulder, as can be expected of the monomer-like absorption of flatly adsorbed, hardly interacting molecules. Upon completion of the first ML the peak shifts by 0.1 eV toward 1.6 eV, indicating a stronger interaction of optical transition dipoles between the stacked layers. However, the spectral line shape is strongly different from triclinic SnPc[36] and resembles that of monoclinic PbPc, which corroborates a similar molecular arrangement as already deduced from LEED measurements.

According to the LEED and DRS results, together with the thickness dependence of the workfunction, we conclude that SnPc on HOPG grows in quasi-one-dimensional columns similar to the monoclinic phase of PbPc single crystals.

It should be noted that the polymorph formed is very sensitive to the growth conditions of the film and the substrate surface. In fact, we sometimes observed films partly featuring broad LEED spots and DRS signatures of a triclinic-like structure. In order to fabricate the quasi-one-dimensional columns consisting of either concave or convex stacking of SnPc molecules, we need the monoclinic film since the triclinic film contains alternative convex and concave molecular packings. As deduced from LEED and DRS results, the as-deposited films consist predominantly of the monoclinic phase while the films annealed beyond 400 K are in the triclinic phase (Figure 3d). Films deposited on substrates kept at higher than room temperature also show the triclinic phase. Thus, the monoclinic phase of SnPc is assumed to be metastable. Fortunately, the line shape of UPS correlates well with the polymorphs (Figure S4 in the Supporting Information) which facilitates a clear distinction. Therefore, in each electron spectroscopy measurement, we confirmed the polymorph of the obtained film from the line shapes of UPS.

3.2. Electronic Structure. After clarifying the structural properties of the SnPc/graphite films, UPS and LEIPS were

DOI: 10.1021/acs.jpcc.8b02581
J. Phys. Chem. C 2018, 122, 12090−12097

applied to examine the occupied and unoccupied energy levels, respectively. Figure 4 shows the spectra of films with

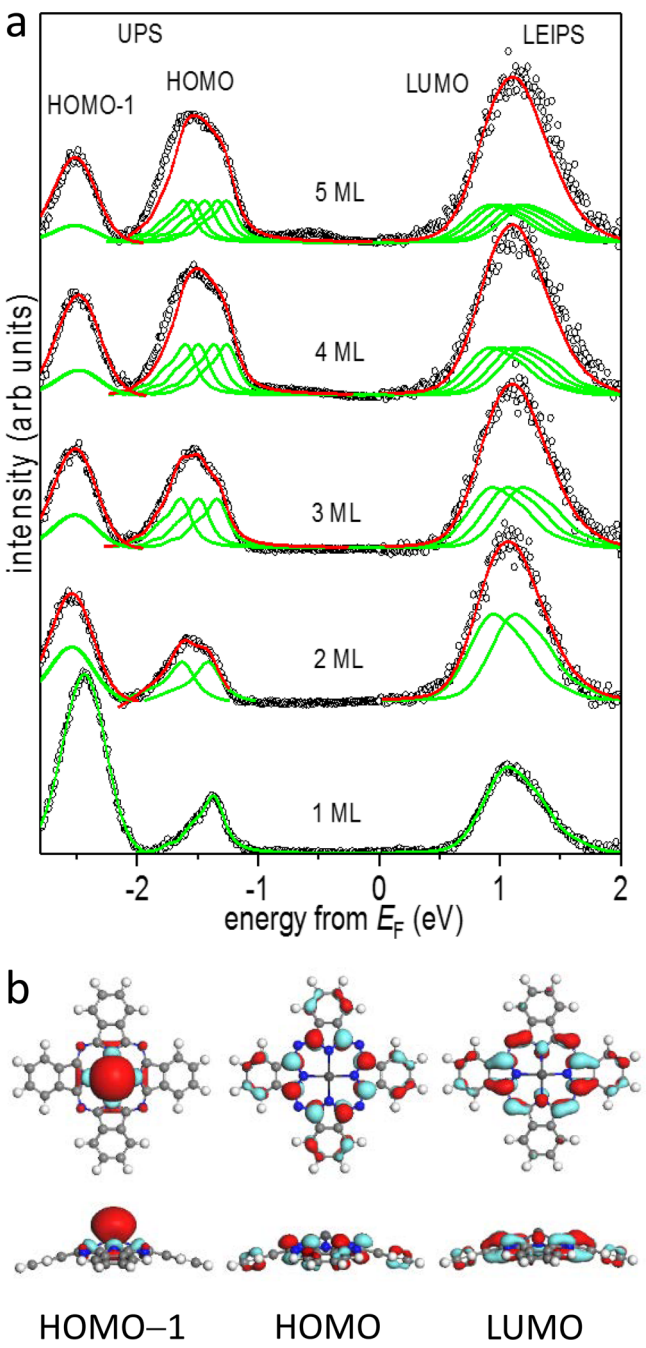

Figure 4. (a) Electronic structure of SnPc films with reference to the Fermi level E_F. (a) The combined UPS and LEIPS spectra of SnPc/HOPG, with the thickness ranging between 1 and 5 ML. The experimental data (open circles) are reproduced with the sum (red lines) of several spectral line shapes of the 1 ML peak (green lines) based on the energy levels calculated by our Hückel model (see Figure 1 and text). (b) Calculated molecular orbitals of SnPc.

thicknesses between 1 and 5 ML and annealed at 373 K. The respective data sets for as-deposited samples are shown in Figure S3 in the Supporting Information. On the basis of the calculated energy levels of a single SnPc molecule belonging to the C_{4v} point group, the peaks observed at −2.4, −1.3, and 1.1 eV are assigned to the HOMO−1 (a_1), HOMO (a_2) and LUMO (e)-derived levels, respectively. As the film thickness increases, the width of each peak also increases.

First, we analyze the difference in the spectra of 1 and 2 ML in detail. As we demonstrated previously in the case of PbPc bilayers on HOPG,[8] we could reproduce each peak of the 2 ML film as the sum of a corresponding peak from the 1 ML film and a slightly shifted copy of it, to mimic an assumed orbital splitting due to intermolecular interaction within molecular dimers. As shown in Figure 4, also the 2 ML spectra of SnPc show excellent agreement with the superposition of two 1 ML spectra with energy separations of 203 (190) and 256 (243) meV for the annealed (as-deposited) HOMO and LUMO, respectively, while the separation is less than 10 meV for the HOMO−1. Assuming the energy splitting is twice the transfer integral t according to the Hückel approximation, we calculated the transfer integrals as $t_{HOMO-1} \leq 5$ meV, $t_{HOMO} = 102$ (95) meV, and $t_{LUMO} = 128$ (122) meV. On the basis of multiple data taken under different experimental conditions, we evaluate the transfer integrals as $t_{HOMO-1} < 5$ meV, $t_{HOMO} = 100$ meV and $t_{LUMO} = 128$ meV, respectively, with uncertainties of 10 meV (see Tables S1 and S2 and associated text in the Supporting Information for the evaluation of the values). Some larger deviation between experimental and fitted spectra, especially noticeable for the larger film thicknesses of the as-deposited films, is most probably caused by the higher degree of disorder. This means in turn that the broadening of the 2 ML spectrum of the annealed film in Figure 4 represents a peak splitting predominantly caused by the intermolecular orbital interaction and not by inhomogeneous broadening which is negligible here (Figure S3 in the Supporting Information).

Now that the transfer integrals along the stacking direction in a dimer are obtained, we will discuss the thickness-dependent spectral line shape for film thicknesses of 3 ML and beyond. As mentioned above, the separations between the energy levels in chains of different numbers of molecules can be calculated as in Figure 1 within the framework of the Hückel approximation. The transfer integral t has been obtained for each orbital from the spectra of the bilayer as outlined above. On the basis of these values, we simulate the spectral line shape as a sum of spectral features of the 1 ML film in Figure 4a. The agreement with the experimental data is excellent in all cases. We emphasize that the only free parameters are the normalization factor of the peak intensity and the center energy of the peak. The relative intensity of the components is kept fixed. The energy separations of the peaks are determined by the Hückel method (Figure 1) using the experimentally determined transfer integrals from the dimers. This finding supports the conclusion that SnPc grows indeed predominantly layer-by-layer in quasi-one-dimensional stacks on HOPG, and the broadening of the peaks is really caused by intermolecular orbital interaction, as the good agreement over the whole range of film thickness cannot be accidental.

Yet, as the film thickness increases (particularly to 4 and 5 ML), certain differences between the modeled and experimental spectra become discernible. SnPc molecules often show island growth in multilayers, that is, Stranski-Krastanov growth.[40−42] Therefore, a commencing inhomogeneity in the film thickness may give rise to the slight disagreement between the simulated and experimental results in multilayers. We also assessed the limitation of the simple Hückel approximation, that is, the neglect of the overlap integral and the inclusion of only the nearest-neighbor transfer integrals. The extended Hückel method including the overlap integral gives essentially

DOI: 10.1021/acs.jpcc.8b02581
J. Phys. Chem. C 2018, 122, 12090−12097

the same energy separations. Because the wave function decays exponentially with the distance, the transfer integral between the next-nearest neighbor molecules should already be negligible, as exemplified by the DFT calculation of pentacene.[7]

Finally, we want to discuss the small transfer integral in the HOMO−1-derived level, which may be surprising at the first glance. Figure 4b shows the molecular SnPc orbitals of the HOMO−1, HOMO, and LUMO as calculated by means of DFT. The HOMO and LUMO are π-orbitals being delocalized over the phthalocyanine ligand, while the HOMO−1 is localized on the metal atom and extends only to the concave side. Consequently, the intermolecular overlap should be much smaller for the HOMO−1 than for both the HOMO and the LUMO in a one-dimensional column. Such differences in the shape of molecular orbitals should also affect the angular dependence of UPS and LEIPS intensities. The HOMO and LUMO intensities increase with the number of layers while the HOMO−1 band's intensity decreases from 1 to 2 ML. This anomaly in the intensities is likely due to the difference in the molecular orientation in 1 ML and the multilayer as discussed above.

Further, the observed transfer integrals are larger for the LUMO than for the HOMO indicating the larger overlap between the LUMOs of nearest-neighbor molecules along the stack compared to the HOMO. Actually, the wave functions of the HOMO and LUMO appear rather similar in terms of the number of nodes in Figure 4b. The calculated bandwidths in Figure 2 are also slightly larger for the LUMO (0.59 eV) than for the HOMO (0.54 eV). This suggests that the spatial extension of unoccupied orbitals is larger due to the smaller shielding of the positive charges of the atomic cores by the valence electrons. Note that the difference in the instrumental resolution does not affect the transfer integrals as discussed in Section 5 of the Supporting Information.

4. CONCLUSION

We successfully prepared layers consisting of quasi-one-dimensional stacks of SnPc on graphitic surfaces with a well-defined number of layers in the range between 1 and 5 ML. We examined the HOMO−1, HOMO, and LUMO-derived energy levels using UPS and LEIPS. The observed evolution of the peak shape and width is interpreted as an orbital splitting caused by intermolecular orbital interaction. The transfer integrals for the HOMO−1, HOMO, and LUMO are determined to be $t_{HOMO-1} \leq 15$ meV, $t_{HOMO} = (100 \pm 10)$ meV and $t_{LUMO} = (128 \pm 10)$ meV, respectively, in the framework of the Hückel approximation which was applied here. The differences in the magnitudes of the transfer integrals can be understood by considering the spatial extension of molecular orbitals.

■ ASSOCIATED CONTENT

Supporting Information

The Supporting Information is available free of charge on the ACS Publications website at DOI: 10.1021/acs.jpcc.8b02581.

DRS raw data; raw UPS and LEIPS spectra and background removal; UPS and LEIPS spectra of as-deposited SnPc/HOPG; SnPc polymorphs and line shapes of UPS; uncertainties in the transfer integrals; effect of the energy resolution of the apparatus on the transfer integrals (PDF)

■ AUTHOR INFORMATION

Corresponding Authors

*(H.Y.) E-mail: hyoshida@chiba-u.jp.
*(S.K.) E-mail: kera@ims.ac.jp.
*(T.F.) E-mail: torsten.fritz@uni-jena.de.

ORCID

Matthias Meissner: 0000-0001-6281-2184
Marco Gruenewald: 0000-0003-1545-7831
Satoshi Kera: 0000-0003-0353-5863
Roman Forker: 0000-0003-0969-9180
Torsten Fritz: 0000-0001-6904-1909
Hiroyuki Yoshida: 0000-0002-8889-324X

Notes

The authors declare no competing financial interest.

■ ACKNOWLEDGMENTS

We thank Mr. Ryo Shiraishi of IMS for his technical assistance in the PbPc band calculation. Computation time was provided by the SuperComputer System, Institute for Chemical Research, Kyoto University. This research was supported by JSPS KAKENHI (Grants 26288007 and 26248062), and was partially founded by the DFG (Grant Numbers FO 770/2-1 and FR 875/16-1).

■ REFERENCES

(1) Coropceanu, V.; Cornil, J.; da Silva Filho, D. A.; Olivier, Y.; Silbey, R.; Brédas, J.-L. Charge Transport in Organic Semiconductors. *Chem. Rev.* **2007**, *107*, 926−952.

(2) Silinsh, E. A. *Organic Molecular Crystals: Their Electronic States*; Springer Series in Solid-State Sciences, Springer: Berlin, 2012; Vol. *16*.

(3) Ueno, N.; Kera, S. Electron Spectroscopy of Functional Organic Thin Films: Deep Insights into Valence Electronic Structure in Relation to Charge Transport Property. *Prog. Surf. Sci.* **2008**, *83*, 490−557.

(4) Yamane, H.; Kosugi, N. Substituent-Induced Intermolecular Interaction in Organic Crystals Revealed by Precise Band-Dispersion Measurements. *Phys. Rev. Lett.* **2013**, *111*, 086602.

(5) Hoffmann, R. *Solids and Surfaces: A Chemist's View of Bonding in Extended Structures*; VCH Publishers: New York, 1988.

(6) Hoffmann, M.; Schmidt, K.; Fritz, T.; Hasche, T.; Agranovich, V. M.; Leo, K. The Lowest Energy Frenkel and Charge-Transfer Excitons in Quasi-One-Dimensional Structures: Application to MePTCDI and PTCDA Crystals. *Chem. Phys.* **2000**, *258*, 73−96.

(7) Yoshida, H.; Sato, N. Crystallographic and Electronic Structures of Three Different Polymorphs of Pentacene. *Phys. Rev. B: Condens. Matter Mater. Phys.* **2008**, *77*, 235205.

(8) Kera, S.; Fukagawa, H.; Kataoka, T.; Hosoumi, S.; Yamane, H.; Ueno, N. Spectroscopic Evidence of Strong π-π Interorbital Interaction in a Lead-Phthalocyanine Bilayer Film Attributed to the Dimer Nanostructure. *Phys. Rev. B: Condens. Matter Mater. Phys.* **2007**, *75*, 121305.

(9) Wang, C.; Dong, H.; Hu, W.; Liu, Y.; Zhu, D. Semiconducting π-Conjugated Systems in Field-Effect Transistors: A Material Odyssey of Organic Electronics. *Chem. Rev.* **2012**, *112*, 2208−2267.

(10) Anthony, J. E.; Facchetti, A.; Heeney, M.; Marder, S. R.; Zhan, X. n-Type Organic Semiconductors in Organic Electronics. *Adv. Mater.* **2010**, *22*, 3876−3892.

(11) Brédas, J.-L.; Cornil, J.; Heeger, A. J. The Exciton Binding Energy In Luminescent Conjugated Polymers. *Adv. Mater.* **1996**, *8*, 447−452.

(12) Knupfer, M.; Fink, J. Frenkel and Charge-Transfer Excitons in C_{60}. *Phys. Rev. B: Condens. Matter Mater. Phys.* **1999**, *60*, 10731−10734.

(13) Djurovich, P. I.; Mayo, E. I.; Forrest, S. R.; Thompson, M. E. Measurement of the Lowest Unoccupied Molecular Orbital Energies

DOI: 10.1021/acs.jpcc.8b02581
J. Phys. Chem. C 2018, 122, 12090−12097

of Molecular Organic Semiconductors. *Org. Electron.* **2009**, *10*, 515−520.
(14) Dose, V. VUV Isochromat Spectroscopy. *Appl. Phys.* **1977**, *14*, 117−118.
(15) Tsutsumi, K.; Yoshida, H.; Sato, N. Unoccupied Electronic States in a Hexatriacontane Thin Film Studied by Inverse Photoemission Spectroscopy. *Chem. Phys. Lett.* **2002**, *361*, 367−373.
(16) Li, Z.; Sun, S.; Li, X.; Schlaf, R. The Impact of Inverse Photoemission Spectroscopy Measurements on Regioregular Poly(3-Hexylthiophene) Films. *Appl. Phys. Lett.* **2014**, *104*, 021606.
(17) Yoshida, H. Near-Ultraviolet Inverse Photoemission Spectroscopy Using Ultra-Low Energy Electrons. *Chem. Phys. Lett.* **2012**, *539*−*540*, 180−185.
(18) Yoshida, H. Measuring the Electron Affinity of Organic Solids: An Indispensable New Tool for Organic Electronics. *Anal. Bioanal. Chem.* **2014**, *406*, 2231−2237.
(19) Yoshida, H. Principle and Application of Low Energy Inverse Photoemission Spectroscopy: A New Method for Measuring Unoccupied States of Organic Semiconductors. *J. Electron Spectrosc. Relat. Phenom.* **2015**, *204*, 116−124.
(20) Boudaiffa, B.; Cloutier, P.; Hunting, D.; Huels, M. A.; Sanche, L. Resonant Formation of DNA Strand Breaks by Low-energy (3 to 20 eV) Electrons. *Science* **2000**, *287*, 1658−1660.
(21) Yoshida, H. Note: Low Energy Inverse Photoemission Spectroscopy Apparatus. *Rev. Sci. Instrum.* **2014**, *85*, 016101.
(22) Sojka, F.; Meissner, M.; Zwick, C.; Forker, R.; Fritz, T. Determination and Correction of Distortions and Systematic Errors in Low-Energy Electron Diffraction. *Rev. Sci. Instrum.* **2013**, *84*, 015111.
(23) Forker, R.; Gruenewald, M.; Fritz, T. Optical Differential Reflectance Spectroscopy on Thin Molecular Films. *Annu. Rep. Prog. Chem., Sect. C: Phys. Chem.* **2012**, *108*, 34−68.
(24) Forker, R.; Fritz, T. Optical Differential Reflectance Spectroscopy of Ultrathin Epitaxial Organic Films. *Phys. Chem. Chem. Phys.* **2009**, *11*, 2142−2155.
(25) Sojka, F.; Meissner, M.; Zwick, C.; Forker, R.; Vyshnepolsky, M.; Klein, C.; Horn-von Hoegen, M.; Fritz, T. To Tilt or Not to Tilt: Correction of the Distortion Caused by Inclined Sample Surfaces in Low-Energy Electron Diffraction. *Ultramicroscopy* **2013**, *133*, 35−40.
(26) The software "LEEDLab" version 1.64 is commercially available from ScientaOmicron at http://www.scientaomicron.com/en/products/350/1155.
(27) Ukei, K. Lead Phthalocyanine. *Acta Crystallogr., Sect. B: Struct. Crystallogr. Cryst. Chem.* **1973**, *29*, 2290−2292.
(28) Iyechika, Y.; Yakushi, K.; Ikemoto, I.; Kuroda, H. Structure of Lead Phthalocyanine (Triclinic Form). *Acta Crystallogr., Sect. B: Struct. Crystallogr. Cryst. Chem.* **1982**, *38*, 766−770.
(29) Frisch, M. J.; Trucks, G. W.; Schlegel, H. B.; Scuseria, G. E.; Robb, M. A.; Cheeseman, J. R.; Scalmani, G.; Barone, V.; Mennucci, B.; Petersson, G. A.; et al. *Gaussian 09*, rev. A. 02.; Gaussian Inc.: Wallingford, CT, 2009.
(30) Miyamoto, A.; Nichogi, K.; Taomoto, A.; Nambu, T.; Murakami, M. Structural Control of Evaporated Lead-Phthalocyanine Films. *Thin Solid Films* **1995**, *256*, 64−67.
(31) Kim, T.-M.; Kim, H. J.; Shim, H.-S.; Choi, M.-S.; Kim, J. W.; Kim, J.-J. The Epitaxial Growth of Lead Phthalocyanine on Copper Halogen Compounds as the Origin of Templating Effects. *J. Mater. Chem. A* **2014**, *2*, 8730−8735.
(32) Friedel, M. K.; Hoskins, B. F.; Martin, R. L.; Mason, S. A. A New Metal(II) Phthalocyanine Structure: X-ray and Mössbauer Studies of the Triclinic Tin(II) Phthalocyanine. *J. Chem. Soc. D* **1970**, *0*, 400−401.
(33) Walzer, K.; Hietschold, M. STM and STS Investigation of Ultrathin Tin Phthalocyanine Layers Adsorbed on HOPG(0001) and Au(111). *Surf. Sci.* **2001**, *471*, 1−10.
(34) Lackinger, M.; Hietschold, M. Determining Adsorption Geometry of Individual Tin-Phthalocyanine Molecules on Ag(111) - a STM Study at Submonolayer Coverage. *Surf. Sci.* **2002**, *520*, L619−L624.
(35) Schwarz, F.; Wang, Y. F.; Hofer, W. A.; Berndt, R.; Runge, E.; Kröger, J. Electronic and Vibrational States of Single Tin-Phthalocyanine Molecules in Double Layers on Ag(111). *J. Phys. Chem. C* **2015**, *119*, 15716−15722.
(36) Gruenewald, M.; Peuker, J.; Meissner, M.; Sojka, F.; Forker, R.; Fritz, T. Impact of a Molecular Wetting Layer on the Structural and Optical Properties of Tin(II)-Phthalocyanine Multilayers on Ag(111). *Phys. Rev. B: Condens. Matter Mater. Phys.* **2016**, *93*, 115418.
(37) Vasseur, K.; Broch, K.; Ayzner, A. L.; Rand, B. P.; Cheyns, D.; Frank, C.; Schreiber, F.; Toney, M. F.; Froyen, L.; Heremans, P. Controlling the Texture and Crystallinity of Evaporated Lead Phthalocyanine Thin Films for Near-Infrared Sensitive Solar Cells. *ACS Appl. Mater. Interfaces* **2013**, *5*, 8505−8515.
(38) Mohan Kumar, T. M.; Achar, B. N. Synthesis and Characterization of Lead Phthalocyanine and its Derivatives. *J. Organomet. Chem.* **2006**, *691*, 331−336.
(39) Kawakita, N.; Yamada, T.; Meissner, M.; Forker, R.; Fritz, T.; Munakata, T. Metastable Phase of Lead Phthalocyanine Films on Graphite: Correlation between Geometrical and Electronic Structures. *Phys. Rev. B: Condens. Matter Mater. Phys.* **2017**, *95*, 045419.
(40) Wang, S. D.; Dong, X.; Lee, C. S.; Lee, S. T. Orderly Growth of Copper Phthalocyanine on Highly Oriented Pyrolytic Graphite (HOPG) at High Substrate Temperatures. *J. Phys. Chem. B* **2004**, *108*, 1529−1532.
(41) Vearey-Roberts, A. R.; Steiner, H. J.; Evans, S.; Cerrillo, I.; Mendez, J.; Cabailh, G.; O'Brien, S.; Wells, J. W.; McGovern, I. T.; Evans, D. A. Growth and Morphology of SnPc Films on the S-GaAs(001) Surface: A Combined XPS, AFM and NEXAFS Study. *Appl. Surf. Sci.* **2004**, *234*, 131−137.
(42) Kim, H. J.; Shim, H.-S.; Kim, J. W.; Lee, H. H.; Kim, J.-J. CuI Interlayers in Lead Phthalocyanine Thin Films Enhance Near-Infrared Light Absorption. *Appl. Phys. Lett.* **2012**, *100*, 263303.

DOI: 10.1021/acs.jpcc.8b02581
J. Phys. Chem. C 2018, 122, 12090−12097